Compressive strength measurements in aluminum for shock compression over the stress range of 4–22 GPa

H. Huang and J. R. Asay[a)]
Institute for Shock Physics and Department of Physics, Washington State University, Pullman, Washington 99164-2816

(Received 3 March 2005; accepted 21 June 2005; published online 10 August 2005)

Measurements of the high-pressure compressive strength are presented for several aluminum alloys shocked to 22 GPa. Five well-characterized aluminum materials were studied, including 6061 alloy with three average grain sizes (50, 30, and <5 μm), pure aluminum 1060 (99.5% Al) with a 180-μm grain size, and ultrapure aluminum (99.9998% Al) with a 300-μm grain size. The purpose of these experiments was to investigate deformation mechanisms responsible for the apparently anomalous quasielastic recompression previously observed and to determine how the shock-induced yield strength varies with initial properties. The yield strength was estimated using combined reshock and release techniques previously developed. These results show that quasielastic recompression occurs for all materials investigated and is independent of grain size and impurity level. The shear stress and the shear strength at the shocked state were estimated from the reshock and release wave profiles. These results are consistent with previous investigations and suggest that the shear stress at the Hugoniot state is less than the yield strength. This is thought responsible for the observed quasielastic recompression. The present data, together with other reported measurements, illustrate that the yield strength of aluminum increases with applied shock stress to 90 GPa. The Steinberg-Guinan strength model [Steinberg, Cochran, and Guinan, J. Appl. Phys. **51**, 1498 (1980)] was used to describe these data and was found to represent the overall data trend with increasing stress, but is not an accurate representation. The collective data suggest that the increase in strength at shock states, $\Delta Y(\Delta Y = Y_{\text{yield}} - Y_{\text{HEL}})$, increases with applied stress and plastic strain. A strength model was developed to describe this increase, which fits the data accurately to 55 GPa and reveals that ΔY increases with shock stress in three distinct regions. It also strongly indicates that metallurgical properties, such as impurities and grain size, influence the ambient yield strength, but not the change in strength, which appears to be controlled by the shock-deformed aluminum matrix and possibly grain boundaries. © *2005 American Institute of Physics*. [DOI: 10.1063/1.2001729]

I. INTRODUCTION

Shock wave investigations have been used for several decades to study the dynamic response of materials. Early studies were directed to studies of the equation of state (EOS) in regimes inaccessible by other methods.[1] Principal data obtained in these studies involved measurement of shock and particle velocities, which were used to deduce EOS properties. With the advent of time-resolved diagnostic methods, a large number of thermomechanical and physical properties of materials have been studied, including a variety of phase transitions, electrical properties, nonlinear elastic response, and dynamic failure.[1,2] These techniques have been especially useful for studying mechanical properties such as compressive stress under intense shock loading. The study of material strength (ability to support a stress deviator), resulting in a constitutive description for the deviatoric stress state of materials subjected to uniaxial strain by shock loading, is important for understanding deformation mechanisms, both for identifying the responsible physical, chemical, and material properties and for describing material science effects. Fowles quantified the relationship between bulk material response and the deviatoric states achieved by uniaxial compression and presented a technique for estimating the compressive strength through comparison of uniaxially compressed states with hydrostatic compression.[3] This method provides a straightforward way to determine shock-induced material strength from a comparison of the Hugoniot stress and the hydrostatic pressure, but is practically limited to low shock levels. Since this early work, a variety of other methods have been developed for studying compressive strength in the shock-compressed state.

Asay and co-workers developed a wave profile technique, referred to as the self-consistent method,[4–6] for estimating compressive strength under shock loading. In this technique, measurement of the unloading and reloading wave profiles from the initial shock state is used to estimate both the hydrodynamic and deviatoric responses, using rather simple assumptions about the elastic-plastic response. This work not only provided the shear stress and strength at the shocked state in an aluminum alloy, 6061-T6, but also demonstrated that the material exhibited anomalous elastic-like loading, which results from initial elastic material response followed by a mixed elastic-plastic deformation and referred to as quasielastic loading produced by subsequent shock loading from the shock state at sufficiently high-stress levels.[4–6] The quasielastic deformation observed during re-

[a)]Electronic mail: jrasay@wsu.edu

shocking suggested that either the material exhibited time-dependent yield behavior for shock stresses exceeding ~10 GPa, resulting in quasi-elastic-plastic response,[7,8] or that the average shear stress state induced by initial shock loading differs from the critical shear strength.[4] These experiments, as well as experiments on other materials, also showed that the compressive yield strength increased significantly with the applied shock stress.[9–14] The quasielastic response upon reshock was also found in other metals, such as tungsten[9] and beryllium[15] and in ceramics, such as alumina[16] and boron carbide.[10]

Other time-resolved methods have been developed for probing the compressive strength of shocked materials, including compression-shear techniques,[17,18] and lateral-longitudinal stress measurements.[12,19–22] Except for the work of Al'tshuler *et al.*, these methods have not been used to study recompression from the shocked state. Most recently, a Rayleigh-Taylor instability method has been developed for studying compressive strength under shockless loading to ultrahigh pressures.[23] Chartagnac has summarized the various methods used for compressive strength measurements under shock loading,[24] and Moss has generalized the self-consistent method to general assumptions of the flow behavior, including kinematic hardening.[25]

The observation of quasielastic response from an initial shocked state raises several questions about the dynamic flow process. The established mathematical formalisms for elastic-plastic flow predict that further compression from a shocked state in the plastic regime should produce plastic flow unless the material exhibits rate-dependent elastic response. The early experiments by Asay and co-workers[4,5] indicated that this was not the case for the aluminum material they studied and they further showed that standard rate-dependent material models would not explain the effect. Based on the quasielastic reshock behavior observed in these experiments, two explanations have been advanced. Swegle and Grady[7] proposed that at higher shock levels the strain rates produced by the first shock induce localization of dissipative energy on a submicron scale, resulting in small heterogeneities or microshear bands with local temperatures approaching melting. After shock passage, a rapid cooling of these local hot spots is achieved through thermal equilibrium with the surroundings. In their model, the yield strength and resolved shear stress dropped precipitously during the rise of the shock wave, with the yield strength recovering before the application of the reloading shock. In this way, the recovery of the strength and the resulting low resolved shear stress in the first shocked state results in a time-dependent yield strength and the quasielastic recompression observed before the arrival of the second plastic shock. The constitutive model which they formulated was found to accurately model the experimental data.

Another mesoscale model was proposed by Lipkin and Asay[4] for describing the observed response. They assumed that planar loading of a polycrystalline material induces multiple wave interactions on a local scale, resulting in localized variations in stress, density, and temperature that could produce relaxation of the resolved shear stress at various locations within the grain structure. A variety of material effects could cause this, including variations in grain orientations with resulting variations in elastic and plastic responses, shear stress distributions produced during material fabrication, local imperfections such as inclusions, microporosity resulting in local wave interactions, and possibly other unknown heterogeneities. Some of these effects were observed by Meyers and Carvelho in the late 1970s, who predicted variations in state variables produced by shock loading through the use of two-dimensional (2D) numerical simulations.[26] Lipkin and Asay[4] developed a continuum-level model for quantitatively explaining these variations, by assuming that all variables, including the resolved shear stress, could be represented by an average over the fluctuations induced at the grain scale and a deviation from the average described by a Gaussian function. The model assumed that there is a distribution of shear stress states produced after shock compression with some fraction of the states less than the critical shear stress. For states of shear stress at localized regions that lie within the yield surface, elastic recompression will occur until the local yield stress is achieved. The collective response of the material will thus exhibit a combination of elastic and plastic deformation responses, resulting in the so-called quasi-elastic-plastic compression. Lipkin and Asay found that this model could also reproduce the experimental data.[4] Recently, the distributed shear stress approach was formulated into a more rigorous elastic-plastic model by Vogler and Asay who found that a common distribution function could accurately describe combined unloading and reloading data.[27]

These two different physical models equally describe the observed continuum response for completely different localization processes and illustrate the problem of obtaining unique interpretations using continuum data alone, because of the highly complex nature of the shock process. In order to resolve this issue and to possibly identify the correct mesoscale deformation mechanisms, carefully controlled shock wave experiments need to be performed on materials with different initial metallurgical properties for a variety of loading conditions, the continuum properties sensitive to these property changes should be precisely measured, and time-resolved *in situ* diagnostics for probing local deformations should be developed. This focused approach would allow correlations between the mesoscale properties, such as grain size, grain distributions, and impurity states with macroscopic observables, such as compressive strength in the shocked state. In this regard, the previously observed quasi-elastic recompression response from the shocked state serves as a useful metric for identifying the sensitivity of continuum response to mesoscale deformations if a correlation can be established with metallurgical properties that produce these deformations. This would be critical to understanding the problem and would be invaluable for differentiating between various mesoscale models proposed to explain the continuum response.

We have initiated research to systematically study the relationship between metallurgical properties and the mechanical response of strongly shocked materials in order to provide more information about mesoscale mechanisms responsible for the observed continuum response. In this paper,

we present shock wave studies on a variety of aluminum materials, including pure aluminum and several aluminum alloys to address the issues discussed earlier; i.e., how do initial metallurgical properties influence mesoscopic deformations leading to the observed continuum measurements of compressive strength in the shocked state? In these experiments, a combination of unloading and reloading wave profile experiments was conducted. Commercially available 6061-T6 aluminum alloy was selected for the studies of grain-boundary variations and the effects of impurity inclusions on dynamic response, because of the large body of previous shock experiments on this material.[4–6] Toward this end, we have carried out an in-depth investigation on well-characterized Al samples: 6061-T6 Al with average grain sizes of approximately <5, 30, and 50 μm; pure Al 1060 (average grain size of 180 μm and purity of 99.5%); and ultrapure Al (average grain size of 300 μm and purity of 99.9998%). For these different materials, experiments were conducted for the first shock states of nominally 4, 13, and 22 GPa. The combination of unloading and reloading profile measurements from these states allows estimation of the yield strength in the shocked state, as will be shown. The study of materials with different metallurgical properties allows determination of the importance of grain effects on the dynamic strength for grain sizes ranging from a few microns to several hundreds of microns, evaluation of whether inclusions have a notable effect on compressive strength, and how these material effects influence the quasielastic recompression.

The self-consistent method was used to estimate the shear stress τ_H and the shear strength τ_c at the shocked state. The present results are consistent with the previous strength measurements in aluminum[6,28,29] in that the shock-induced shear strength or equivalently the yield strength is found to significantly increase over the shock stress range studied. A major observation is that the change in compressive yield strength, i.e., Y-Y_0, is similar for all materials studied, irrespective of initial metallurgical properties, such as grain size. This result suggests that shock-induced deformation dominates compressive strength under high rate loading, while metallurgical properties are important to initial deformation properties at lower loading rates, as is well established.

The present studies have elucidated several additional observations. Quasielastic response during recompression from the shocked state is observed at all stress levels for all materials studied. Since the ultrapure material contains only minute amount of impurities and the data agree with those on 6061 alloy, the present results indicate that the main contribution to quasielastic response observed during recompression from the shock state is from grain-boundary interactions and not from impurities or inclusions in the materials. The effect of localized thermal heating resulting in a time-dependent yield behavior as previously discussed[7] cannot be ruled out from the present data. Experiments on single-crystal aluminum, which are planned in future experiments, will be necessary to resolve this question.

Although the major goal of this study was to experimentally evaluate the high-pressure compressive strength, the Steinberg-Guinan strength model,[30,31] which is commonly used for comparing with shock wave profile data on metals, was carefully compared with the experimental data. The comparison shows that the model describes the general stress dependence of the yield strength but overestimates the compressive strength at lower stress levels and underestimates it at higher stresses. A strength model was developed to describe the increase in yield strength for all materials studied, including yield strength data on 2024 and duraluminum at shock stresses to 90 GPa.[28,29] The model describes the increase in yield strength versus the normalized yield strength, although the functional form for the plastic strain dependence had to be significantly modified to more accurately represent the experimental data. This model accurately simulates all reported strength data to 55 GPa and shows that the shock-induced strength has work hardening (plastic strain), pressure hardening, and temperature softening components, as also given by the Steinberg-Guinan model. A future paper will describe this model in more detail, including a discussion of specific deformation mechanisms that could account for the experimental observations, although it is presented here for comparison to experimental data.

In the following, we will briefly describe the aluminum materials studied, the experimental technique for estimating compressive strength, the results of all experiments (about 23), and present a discussion of the strength model used to describe the data obtained in the present work and also data obtained at higher shock stresses.[28,29]

II. EXPERIMENTAL METHOD

A. Aluminum materials

1. Pure aluminum (99.5% and 99.9998%)

a. 1060 aluminum The pure aluminum samples studied were prepared from commercially available 1060 aluminum alloy (Reynolds Aluminum Company, Richmond, Virginia). This material has a total impurity level of 0.4%, with principal impurities of Fe (<0.35 wt %), Cu (<0.05 wt %), Si (<0.05 wt %), Ti (<0.007 wt %), and 5-ppm H_2. The microhardness was 20.5 ± 0.6. The grain size was determined with the electron backscattering diffraction (EBSD) technique.[32] A typical result is shown in Fig. 1. Transmission electron microscopy (TEM) measurements indicated an approximately equiaxed dislocation cell structure with a mean size in the range of 2–2.5 μm and a dispersion of fine dislocation loops.[33]

b. Ultrapure aluminum Ultrapure aluminum was obtained from Alfa Aesar Inc. in the form of either rod or plate stock with principal impurities of O (<11 ppm), N (<5 ppm), C (<2.5 ppm), and 4-ppm H_2. The hardness values were 19.4 ± 1.2 and 19.7 ± 0.4, respectively. ESBD measurements indicated an average texture of 10.8, and a grain distribution that varied considerably over different positions in the sample. The average grain size by number density was about 300 μm.

2. 6061 aluminum alloy

A principal goal of these experiments was to determine effects of grain-size variation, with other metallurgical properties held constant. A 6061 aluminum alloy, which had com-

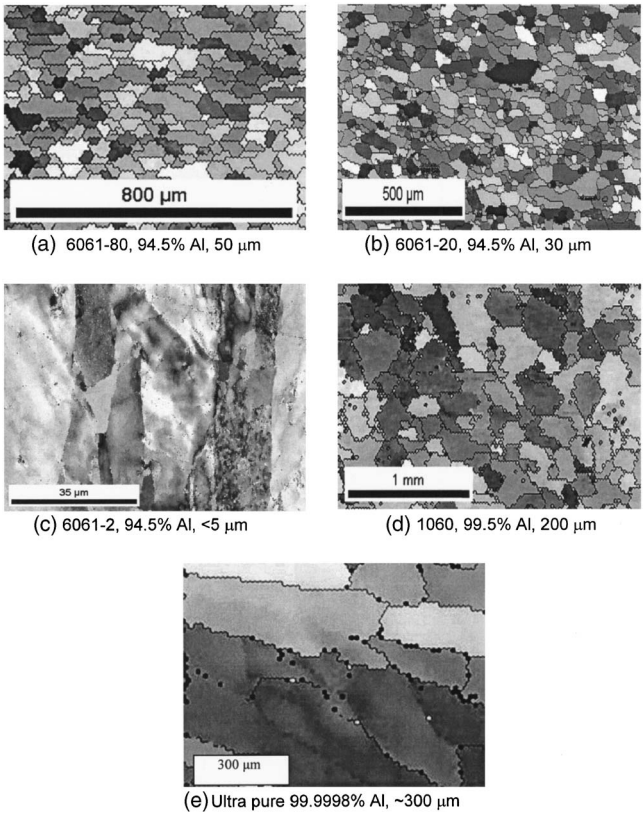

FIG. 1. EBSD and purity data for the five aluminum materials tested.

positions of >94.5 wt % Al, 1.1 wt % Mg, 0.68 wt % Si, 0.16 wt % Cr, 0.49 wt % Fe, and 0.38 wt % Cu, was used for this purpose. A combination of mechanical rolling followed by heat treatment was followed in order to achieve the desired grain sizes and to attempt achieving the T6 hardened condition. A kinetics study of grain-size variation versus time and temperature was first performed and used to extrapolate the resulting grain growth curves for the specific grain size desired.[34] This process held rolling deformation constant at 50% reduction and the time and temperature were varied in specific increments to achieve the desired grain size. For samples to be used in the shock wave experiments, plates of as-received 6061-T6, 25 mm thick and about 75 mm in square dimension, were used as starting material for the rolling and temperature processing. After the grain size was achieved, the plates were heat treated as follows: sample set designated as 6061-02, 400 °C for 1 h; sample set 6061-20, 550 °C for 1 h; and sample set 6061-80, 600 °C for 1 h. Following the heat treatment, the samples were water quenched followed by aging at 160 °C for 18 h. Prescribed thermal treatments for the preparation of 6061-T6 alloy were followed to minimize residual strain produced during mechanical deformation, although EBSD measurements revealed more texture for the smaller grained materials possibly resulting in more residual strain.

Although the goal was to obtain the T6 heat treatment for the different grain sizes, metallurgical examination after processing revealed deviations from this, especially for the small grain sizes. The initial properties of each group are briefly described in the following, using designations intended for the grain sizes; e.g., 6061-80 indicates a desired grain size of 80 μm.

a. 6061-02 EBSD indicated well-defined grains of differing crystal orientations that were not fully established and with more of a subgrain structure. The average subgrain size was found to be less than 5 μm. The texture determined from EBSD was 6.9, indicating a strong nonisotropic grain distribution. Rockwell A hardness (60-kg load) was 13.5 ± 0.5 and the microhardness was 59.4 ± 1.8. These values are lower than the stock material indicating that the samples were likely in an overaged condition. TEM indicated significant dispersion of constituent particles consisting of Al–Fe and/or Al–Fe–Si in the form of intermetallic rods and cuboids in the size range of 0.08–0.4 μm. The matrix between the constituent particles was found to be characterized by a fine, diffuse dislocation cell structure comprised of tangled dislocation walls on the order of 0.1-μm size and contained dislocation loops.

b. 6061-20 The average grain size by number density was about 30 μm, and about 60 μm by areal density. The texture was 2.936 for (100) ⟨110⟩ in the cross-sectional direction. Rockwell A and microhardness values were (60 kg) of 28 ± 0.5 and 80.7 ± 0.6, respectively, which are lower than those for stock 6061-T6.

TEM showed a similar constituent particle distribution to 6061-02. Very coarse, blocky particles were observed with sizes in the range of 3–5 μm. A tangled dislocation cell substructure was also observed with evidence of directionality in the dislocation tangles and appearance of band formation with a spacing of about 0.5 μm.[33]

c. 6061-80 The average grain size by number density was about 50 μm, and about 60 μm by areal density. The texture was found to be 1.753 (100) in the cross-sectional direction and 2.326 (100) in the plane view, which is closer to an isotropic distribution. Hardness measurements showed a Rockwell A (60 kg) of 39.5 ± 0.5, and a microhardness of 108.4 ± 1.4, which are essentially equal to those for stock 6061-T6. However, the grain size was considerably lower than the 6061-T6 alloy previously studied.[6]

TEM and optical microscopy indicated a fine constituent particle distribution and also coarse, blocky particles. The dislocation substructure was significantly different from the other two 6061 materials in that intersecting bands of dislocations were observed that crossed grain boundaries. High magnification imaging showed that the bands were comprised of tangled dislocations that contained long straight segments of parallel dislocations. Crystallographic trace analysis indicated that the bands were parallel to intersecting {111} planes. These long straight dislocations are consistent with perfect screw dislocations.[33] The density and sound speed for each material are summarized in Table I.

B. Experimental technique

Plate impact experiments were performed using either a 100-mm-diameter light gas gun or a 30-mm-diameter powder gun.[35] The impact velocity for the gas gun experiments was measured to within 0.25% using a series of electrical

TABLE I. Summary of density, sound speed, Hugoniot elastic limit (HEL), and yield strength (Y_0) of various aluminum materials.

	6061-02	6061-20	6061-80	Ultrapure Al	1060 Al
Density (g/cm^3)	2.70±0.01	2.70±0.01	2.70±0.01	2.70±0.01	2.71±0.01
Sound speed (km/s)	6.43±0.02	6.43±0.02	6.44±0.02	6.46±0.02	6.46±0.02
HEL (GPa)	0.26	0.35	0.63	0.15	0.12
Y_0 (GPa)	0.13	0.18	0.32	0.07	0.06

shorting pins. The impact velocity measurement in powder gun experiments incorporated a laser beam interrupt system with an accuracy of about 0.5%.

The experimental configuration used for the reshock and release experiments is shown in Fig. 2. To achieve the stress range of interest and maintain well-defined initial planar shock loading followed by either planar unloading or planar reloading, two types of impact configurations were used. At the initial impact level of 4 GPa, *z*-cut quartz impactors were used along with *z*-cut quartz (Boston Piezo-Optics, Inc.) interferometer windows to measure the wave profiles. *Z*-cut quartz has an elastic limit of about 6 GPa, so that both the initial stress loading of 4 GPa and subsequent recompression to about 6 GPa are elastic. This makes the analysis of both unloading and reloading simpler, since the loading time duration can be accurately predicted, making analysis of wave velocities in the sample straightforward. The *z*-cut quartz impactors were backed by either a free surface over the central area to produce full unloading or by a copper backing [oxygen-free high conductivity (OFHC)] to produce recompression from the shocked state. Solid phase indium bonds of about 4-μm total thickness[9] were used to minimize perturbations in the recompression profile.

For impact stresses of nominally 13 and 22 GPa, symmetric aluminum impactors were used with ultrapure LiF [100] interferometer windows (Saint-Gobain Crystals, Inc., Solon OH 44193). LiF is a widely used window material because of its known mechanical and optical properties and has slightly lower impedance than aluminum over the stress range to 22 GPa. Because of its lower impedance, release wave perturbations from the target/window interface back into the shocked target are small so that corrections necessary to estimate *in situ* wave profiles are small. At the higher impact stresses, the elastic precursor in aluminum is essentially overdriven (completely overdriven for the 22-GPa case), so that both sharp unloading and reloading were induced in the samples. For unloading experiments, a Lexan backing to the Al impactor was used. For reshock experiments, OFHC copper bonded to the Al with indium was used to increase the stress level by about 50% from the initial state. For both the *z*-cut quartz and the LiF window experiments, the optical correction factors, $\Delta\nu/\nu_0=0.081\,07$ for *z*-cut quartz, reported by Jones and Gupta[36] and $\Delta\nu/\nu_0=0.2566+0.0226u_p$ for LiF [100] measured by Wise and Chhabildas[37] were used.

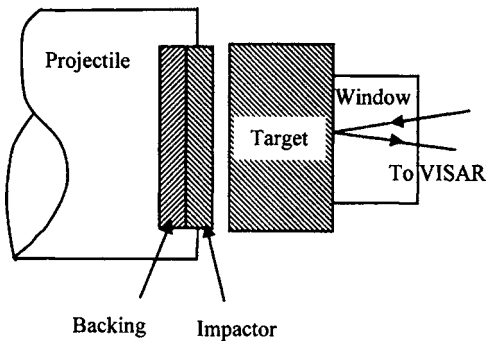

FIG. 2. Experimental configuration for the reshock and release shock experiments.

The velocity interferometer system for any reflector[38,39] (VISAR) was used to measure the time-resolved particle velocity at the window-sample interface, as in the previous reshock and release experiments.[4–6] This system provides good time resolution to address the quasielastic recompression issue. It also provides accurate measurement of longitudinal stress σ_x in the shocked state, since the shock Hugoniot of LiF is accurately known. A disadvantage is that other components of the stress tensor, such as the lateral stress, σ_y or σ_z ($\sigma_z=\sigma_y$), desired for investigation of strength properties, cannot be directly measured. Lateral stress gauges are often used for this purpose.[12,18–22] However, these gauges do not have the time response of the VISAR, which is essential for detecting the anomalous recompression effects. The velocity sensitivity used for the VISAR in all experiments was 0.104 km/s and the time delay (response time) was 1.91 ns. This results in a particle velocity accuracy of 0.2%–1%,[38] depending on actual velocity. The corresponding time resolution was limited by the recording oscilloscopes to ±1 ns.

III. EXPERIMENTAL RESULTS

The experimental results are summarized in Table II. Sample thickness for the corresponding pair of reshock and release experiments was kept as similar as possible in order to perform the stress analyses described later. Since the impedance of *z*-quartz, LiF (100) and aluminum differ slightly, an incremental impedance-matching technique[4] was used to estimate *in situ* profiles, which generally resulted in a small correction. The measured velocity profiles were transformed to *in situ* profiles for the aluminum samples based on the known $U_s \sim u_p$ relation for the window materials[36,40] and aluminum.[41,42] Assuming self-similar motion, which will be discussed later, Lagrangian wave velocities C_L were determined from the particle velocity profiles. Using the differential equations of motion, it was then possible to determine the Hugoniot stress σ_H and the engineering strain ε. The stress-strain changes during unloading or reloading from the Hugoniot state were used to estimate changes in shear stress, as we will discuss. The 6061-20 aluminum set, was tested for

TABLE II. Summary of reshock and release experiments.

Expt. No.	V_p[a]	x_2 (w)[b]	x_1 (i)[b]	σ_H[c]	ε_H[d]	C_L[a]	$\tau_c+\tau_H$[c]	$\tau_c-\tau_H$[c]	τ_c[c]	τ_H[c]
RS20-1	0.503	1.651(z)	3.180(z)	4.13	4.99	7.13		0.03	0.12	0.10
RL20-1	0.506	1.641(z)	3.180(z)	4.12	5.03	7.15	0.22			
RS20-2	0.502	5.943(z)	3.203(z)	4.13	4.75	7.16		0.03	0.121	0.10
RL20-2	0.499	5.942(z)	3.200(z)	4.14	4.81	7.17	0.22			
RS20-3	2.36	5.914(LiF)	2.318(Al)	22.35	17.06	10.49		0.37	0.55	0.19
RL20-3	2.36	5.912(LiF)	2.299(Al)	22.39	17.09	10.48	0.74			
RS20-4	1.56	5.924(LiF)	2.339(Al)	13.44	12.24	9.03		0.22	0.33	0.11
RL20-4	1.56	5.927(LiF)	2.337(Al)	13.36	12.29	8.90	0.43			
RS20-5	2.36	1.606(LiF)	2.286(Al)	22.0	16.86	10.34		0.41	0.53	0.12
RL20-5	2.36	1.634(LiF)	2.197(Al)	22.0	16.79	10.35	0.65			
RS02-1	0.505	5.979(z)	3.203(z)	4.18	4.84	7.16		0.03	0.12	0.09
RL02-1	0.499	5.977(z)	3.202(z)	4.13	4.74	7.15	0.21			
RS02-2	2.35	6.001(LiF)	2.419(Al)	22.12	16.91	10.31		0.323	0.49	0.16
RL02-2	2.30	5.917(LiF)	2.419(Al)	21.56	16.65	10.24	0.65			
RS80-1	2.36	6.018(LiF)	2.435(Al)	22.35	17.06	10.52		0.45	0.66	0.21
RL80-1	2.30	5.946(LiF)	2.057(Al)	21.57	16.64	10.28	0.86			
RL80-2	0.66	5.848(z)	3.191(z)	5.594	6.11	7.52	0.36		0.21	0.15[e]
RSAl-1	1.49	5.382(LiF)	2.215(Al)	12.84	11.76	8.92		0.17	0.29	0.12
RLAl-1	1.44	5.329(LiF)	2.318(Al)	12.24	11.64	8.97	0.41			
RLAl-2	2.37	5.903(LiF)	1.785(Al)	22.48	17.12	10.37	0.62		0.45	0.17[e]
RS1060-1	1.61	5.888(LiF)	2.332(Al)	14.02	12.64	9.06		0.16	0.30	0.13
RL1060-1	1.58	5.999(LiF)	2.263(Al)	13.61	12.32	9.20	0.43			
RL1060-2	1.15	5.045(LiF)	1.847(Al)	9.48	0.094	8.48	0.27		0.17	0.11[e]

[a]Projectile velocity V_p and the initial Lagrangian longitudinal wave speed C_L for reshock and release waves are in km/s;.
[b]Target thickness x_2 and impactor thickness x_1 in millimeters. The letters in parentheses designate the type of window and impactor materials used, where z infers z quartz.
[c]The quantities σ_H, $\tau_c+\tau_H$, $\tau_c-\tau_H$, τ_c and τ_H have units of gigapascals.
[d]Engineering strain at the shock state is ε_H $[\varepsilon_H=1-(\rho_0/\rho_H)]$ and expressed as a percentage.
[e]Estimated by either linear interpolation or linear extrapolation of neighboring data.

all three nominal Hugoniot stresses: 4, 13, and 22 GPa, which provides a basis for comparison with other sample groups. The Hugoniot elastic limit (HEL) and initial yield strength of the aluminum materials are summarized in Table I. In the following, direct comparison of velocity profiles for the different materials is first presented, and then a discussion of the shear stress estimates in the shocked state is presented, followed by an error analysis for estimating shear stresses. Following presentation of the experimental results, a discussion of possible strengthening mechanisms for aluminum is given.

A. Reshock and release experiments on 6061-20

First, to demonstrate typical particle velocity profiles, reshock/release experiments obtained on 6061-20 (referred to as RS20 and RL20 in Table II) are plotted in Fig. 3. The initial particle velocity states at the target/window interface for the three experimental groupings are approximately 0.25, 0.8, and 1.2 km/s, which correspond to Hugoniot stresses of about 4, 13, and 22 GPa. For convenience in analysis, the initial shock stress for each reshock/release experimental pair was designed to be identical, although small deviations were observed in practice. The sample dimensions varied only slightly, so there was good agreement in similar, reshock/release wave profile pairs. An important observation is that initial release from the shock states corresponds to a quasielastic, rather than elastic response. This observation is in general agreement with other data on metals.[4,12–14]

Equally important, it is noted that the material shows initial quasielastic reloading, which has a ramp nature before the main plastic recompression. The final amplitude of the quasielastic ramp wave is observed to increase with increas-

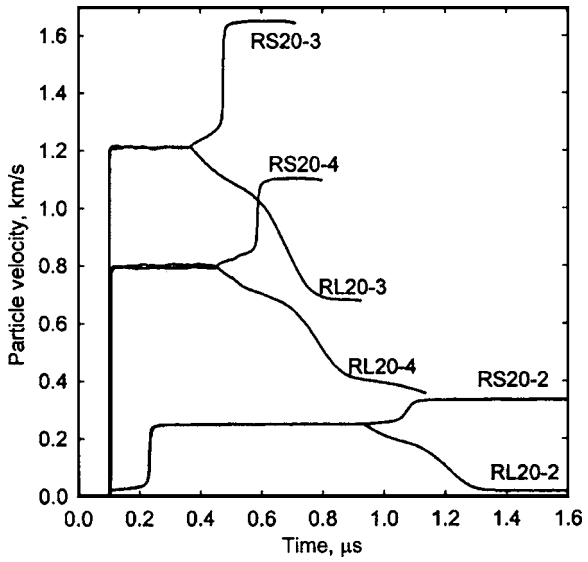

FIG. 3. The particle velocity profiles at the target/window interface for release and reshock experiments on 6061-20.

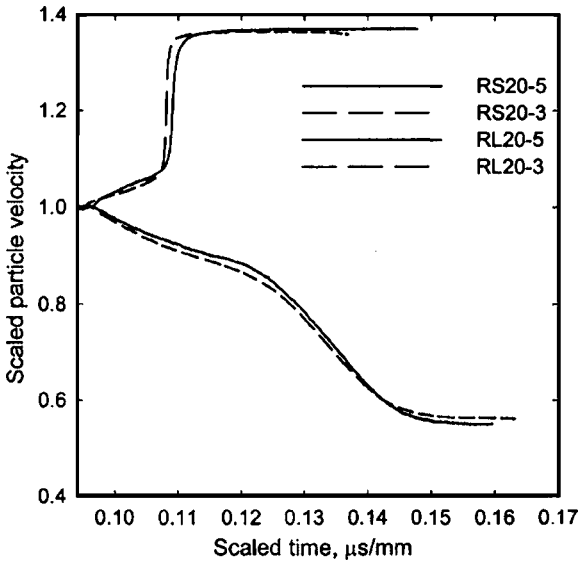

FIG. 4. Self-similar profile comparison for reshock and release waves at 22 GPa. Nominal combined impactor/sample thicknesses for thin and thick pairs were about 4 and 8.2 mm, respectively.

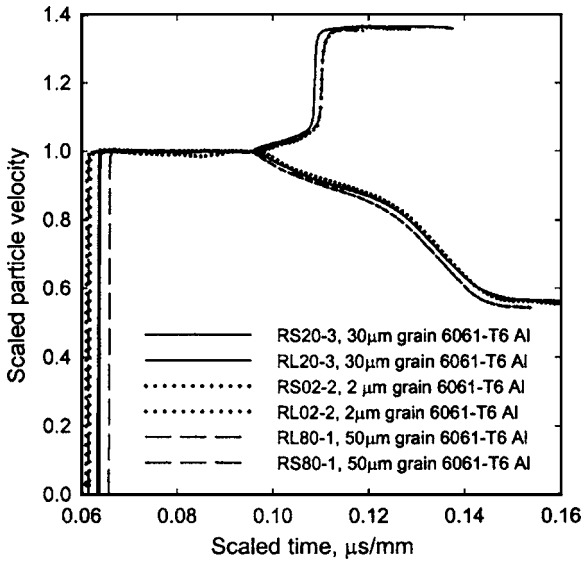

FIG. 5. Comparison of reshock and release experiments on 6061-02 (<5 μm), 6061-20 (30-μm grain size), and 6061-80 (50-μm grain size) at 22 GPa.

ing shock stress. It is approximately 0.01 km/s (4% of impact velocity) for σ_H=4.0 GPa, 0.058 km/s (7.2% of impact velocity) for σ_H=13.2 GPa, and 0.10 km/s (8.33% of impact velocity) for σ_H=22.3 GPa. The results are consistent with previous findings on as-received stock 6061-T6 Al.[6] For reshock and release experiments at a similar shock stress, the initial Lagrangian wave speeds C_L measured for both unloading and reloading are nearly identical with earlier studies.[6] The initial wave speeds, when corrected for density compression, should represent the elastic sound speeds at the corresponding state, but further release is of a quasi-elastic-plastic form, which varies from the normal assumptions used in plasticity analyses. For traditional plasticity, the shock state is usually thought to reside on the yield surface immediately after shock loading so that recompression remains plastic. In this regard, the observed quasielastic recompression represents a departure from the traditional assumptions. The quasielastic response suggests that the aluminum material has either achieved a further ability to support a greater deviatoric stress at a later time after initial shock compression, which would suggest a time-dependent yield behavior, or that the end state of the initial shock compression produces a shear stress state that resides within the yield surface, which would suggest mesoscale deformation effects. These possible effects will be discussed further in a later section.

B. Self-similarity of release and reshock wave profiles

Since sample thicknesses are not identical for the different experiments and it was speculated that the quasielastic response could be a time-dependent effect, two experimental sets were performed on 6061-20 material to test for self-similarity of the reshock and release waves. These experiments, RS20-5 and RL20-5, were conducted on thin samples (less than half of the normal thickness) to compare with the thick samples RS20-3 and RL20-3. The comparison of wave profiles is plotted in Fig. 4, in which particle velocities are normalized by the impact velocity and the time axis is normalized by the combined thickness of the Al impactor and the target. A time shift was also applied to normalize the initial unloading or reloading to the inverse of C_L. Overall, the quasielastic, reshock, and release wave profiles are observed to be similar, but the profiles for the thin samples indicate approximately a 1%–2% slower wave speed. A similar effect is observed in the reshock experiment on the thin sample. These small differences could result from a variety of effects, including observed small differences in the metallurgical properties of the samples, or small effects due to wave perturbations at the LiF window. However, since they are small and on the order of experimental errors, we have assumed that the wave motion is self-similar in the later analyses.

C. Comparison of wave profiles on the samples with different grain sizes

Three corresponding pairs of reshock and release experiments were performed on the three different grain sizes of 6061-T6 alloy for the same nominal Hugoniot stress of 22 GPa. In a later section we will compare our results with those obtained on stock, as-received 6061-T6,[6] which exhibited highly elongated grains with a size ranging to about 500 μm. The normalized wave profiles for the six experiments are plotted in Fig. 5. The comparison shows that both the reshock and release wave profiles are similar, with similar Lagrangian wave speeds. It is noted that overall these profiles are remarkably similar, even with the major differences in sample metallurgy shown in Fig. 1. However, the release wave profile on 6061-80 shows a slightly higher C_L; this alloy, along with 6061-02, also exhibits a slightly higher quasielastic response during reshocking. It will be shown in a later section that shear stresses can be estimated from the wave profiles, so that similar reshock and release wave profiles will result in similar shear stress and yield strength values. The results shown in the figure imply that 6061-80 has a slightly higher shear stress and shear strength at the shocked

state. We will also show later that 6061-80 has a T6 heat treatment based on hardness and HEL measurements comparable to stock 6061-T6 alloy.[6] Figure 5 implies that these materials also have similar yield behavior in the shocked state, even though the grain size varies substantially. These combined results suggest that shock-induced elastic-plastic properties and yield response are relatively independent of grain size for aluminum shocked to high stresses and thus that the well-known Hall-Petch relation,[43] which predicts an inverse square-root relation of yield strength with grain size, apparently does not accurately predict yield properties after shock loading.

Although the T6 condition is not completely satisfied in the 6061-02 and 6061-20 materials studied here, as deduced from the hardness and HEL measurements, the comparable results obtained from the six experiments discussed above and the comparison with stock 6061-T6 aluminum to be discussed later indicate that the quasielastic reshock and release wave profiles are not sensitive to the initial state of heat treatment.

D. Comparison of wave profiles for 6061-T6 alloy with ultrapure Al and the effect of impurity levels

Since grain size is obviously not a critical parameter for quasielastic response, we performed similar experiments to identify other metallurgical effects that could affect mechanical properties after shock compression. For these experiments, we chose pure aluminum samples that do not exhibit precipitation hardening but had varying levels of impurities. These studies included experiments on both commercially pure 1060 and ultrapure aluminum.

Ultrapure aluminum has an initial yield strength of about 0.073 GPa and a Hugoniot elastic limit $\sigma_{\mathrm{HEL}} \approx 0.146$ GPa. The low impurity levels prevent any phase precipitates, as it occurs in the 6061 alloy. As with the case of the 6061 alloy, results show no major difference in quasielastic loading for ultrapure aluminum and 6061-20 samples, even though there is a difference in the grain structure and impurities. Both reshock and release experiments were performed on ultrapure aluminum for an initial shock stress of 13 GPa. The resulting wave profiles are plotted in Fig. 6 in comparison with results from 6061-20 Al for similar initial shock stresses. Although there is no significant difference in the unloading wave profiles, a noticeable lower quasielastic reshock response is observed for the ultrapure aluminum. The slight changes in wave profile histories shown in the figure are due to slight variations in impact velocities, sample thicknesses, and statistical variations in Lagrangian wave velocities.

Despite the fact that the shock stress is slightly lower for the pure aluminum than for 6061-20, the small observed difference in reshock produces a slight difference in the yield behavior and quasielastic response. The relatively good comparison suggests that the major contribution to the observed quasielastic reshock response is not due to precipitates. It is well known that second phase precipitates and impurities have a dramatic effect on mechanical properties under quasistatic loading, but the present results show that this is not the case for shock loading. The observed wave profiles and thus the mechanical behavior under planar shock loading appear to be mainly controlled by the matrix material, i.e., the shock-deformed state of the aluminum material itself and possibly the presence of grain boundaries. It is also well known that the hardening mechanism in 6061-T6 aluminum is due to finely dispersed precipitates, which apparently do not dominate hardening under intense shock loading.

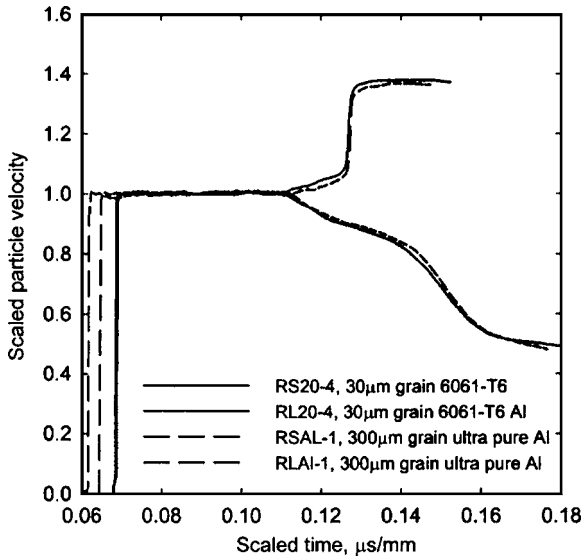

FIG. 6. Comparison of 6061-20 (30-μm grain size) Al alloy and ultrapure Al (99.9998% Al) at 13 GPa to test the combined effect of grain size and precipitate content on wave profiles.

The effect of impurities was also investigated through reshock and release experiments on commercially pure Al 1060 and ultrapure aluminum. The impurity levels of the two materials differ by about a factor of 1000. However, the reshock and release wave profiles are similar, as shown in Fig. 7. The quasielastic reshock response of ultrapure aluminum is observed to be slightly lower than 1060. The 8% lower

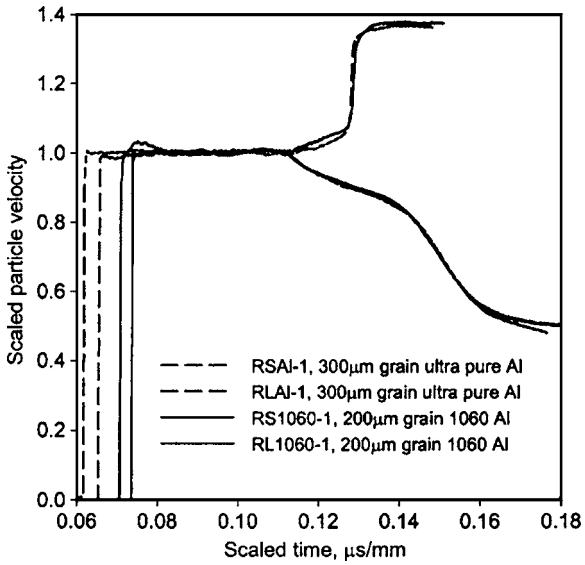

FIG. 7. Comparison of ultrapure Al (99.9998% Al) and pure Al 1060 (99.5% Al) to test the effects of impurity content at 13 GPa. Wave profiles of 1060 Al adjusted by -0.003 μs/mm to correlate with the results on pure Al.

shock stress for the ultrapure aluminum experiments, the lower measured wave speed, and the lower quasielastic reshock stress could result from the lower shock stress. The two sets of experiments on pure aluminum reaffirm that the quasielastic response of aluminum is relatively independent of the impurity level.

E. Estimation of shear stress from longitudinal wave profiles

Because wave profile data do not directly provide measurement of shear stress, it is important to carefully lay out the assumptions used to interpret the data. Although not strictly valid because of deviatoric stresses, it is usually assumed that plastic release from the shocked state can be approximated by hydrostatic response and is isentropic. This is a good assumption for the quasielastic reshock because of the relatively low reshock amplitudes achieved and also for quasielastic release because in both cases the elastic deviators make a relatively low contribution to entropy increase.[44] The assumption of isentropic unloading and reloading is required to estimate shear stress from the measured wave speeds. A concise explanation of the equations for deducing shear stress changes was given in a previous paper.[6] To emphasize the validity of this approach and to clarify the assumptions, a detailed derivation of the shear stress analysis is presented below. The principal assumptions are as follows:

(1) A yield surface exists for the material after shock loading which can be experimentally detected as a transition from quasielastic to plastic response. A related assumption is that the longitudinal stress offset is the same for loading and unloading from the shocked state. Deviation from this assumption leads to error in interpreting the shear stress changes for unloading and reloading.
(2) The yield function Y depends on some measure of plastic strain or/and pressure.
(3) Reloading and unloading from the shocked state are rate independent. A strong rate effect would negate the use of wave profiles to determine Lagrangian wave velocities. Furthermore, strong plastic work hardening during unloading would introduce an error in defining the region of plastic response.

Under uniaxial strain shock loading, the definition of deviatoric stress τ, referred to as the resolved shear stress for convenience, is determined from the difference between the principal stresses in the longitudinal direction σ_x and in the transverse direction σ_y,

$$2\tau = \sigma_x - \sigma_y. \tag{1}$$

The resolved shear stress τ is equal to the shear strength τ_c, $\left(\tau_c = \frac{1}{2}Y_0\right)$, when it reaches the maximum value that the material can withstand.

When the media can support a shear stress, a stress disturbance travels at the local elastic longitudinal wave speed. The Eulerian longitudinal wave speed a under uniaxial strain loading condition is defined for isentropic response as

$$a^2 = -V^2 \left.\frac{\partial \sigma_x}{\partial V}\right|_s, \tag{2}$$

where a is related to the Lagrangian longitudinal wave speed C_L (referred to the original sample dimensions) as

$$\rho a = \rho_0 C_L, \tag{3}$$

since for uniaxial strain loading, the volume change is equal to the dimension change in the longitudinal direction. Engineering strain e is defined in terms of volume change as

$$\varepsilon = \frac{V_0 - V}{V_0} = 1 - \frac{\rho_0}{\rho}, \tag{4}$$

where ρ is the mass density. Differentiating Eq. (4), substituting it into Eq. (2), and applying Eq. (3) result in a differential form for σ_x and ε that can be related to the measured longitudinal wave speed, and thus the longitudinal modulus

$$d\sigma_x = \rho_0 {C_L}^2 d\varepsilon. \tag{5}$$

Equation (5) shows that direct measurement of histories of longitudinal wave speed can provide indirect measurement of changes in the longitudinal stress σ_x for isentropic response defined by Eq. (2). Extension beyond the isentropic assumption will introduce larger error. This equation will be used in this paper for analyzing the quasielastic part of the measured wave profiles.

A similar form for the Lagrangian bulk wave speed C_B can be defined by the following equation when the material has plastically yielded

$$d\bar{\sigma} = \rho_0 {C_B}^2 d\varepsilon, \tag{6}$$

where $\bar{\sigma}$ denotes the mean stress during quasielastic loading (not the Hugoniot mean stress at the shocked state). If work hardening occurs during the incremental strain change, this equation would not be strictly valid for determining the bulk velocity. Differentiating the definition for $\bar{\sigma}$ with respect to engineering strain e provides

$$\frac{d\bar{\sigma}}{d\varepsilon} = \frac{1}{3}\left(\frac{d\sigma_x}{d\varepsilon} + 2\frac{d\sigma_y}{d\varepsilon}\right). \tag{7}$$

Applying Eq. (1), substituting Eqs. (5) and (6) into Eq. (7), and rearranging provides a differential form for the shear stress during quasielastic deformation[6]

$$d\tau = \frac{3}{4}\rho_0 ({C_L}^2 - {C_B}^2) d\varepsilon. \tag{8}$$

Equation (8) shows that changes in the shear stress during isentropic loading in the quasielastic profiles can be obtained by measuring the longitudinal and bulk wave speeds in the appropriate regions of the profiles. The high accuracy and temporal resolution of the VISAR allow accurate wave velocity measurements and thus makes this a practical approach.

The reshock and release experiments provide two independent integration paths for applying Eq. (8). In Fig. 8, the release wave speed C_L which initiates at the Hugoniot state $(\sigma_x, \varepsilon_H, \tau_H)$ in experiments RL20-3 and RS20-3 is observed to decrease with decreasing engineering strain ε during un-

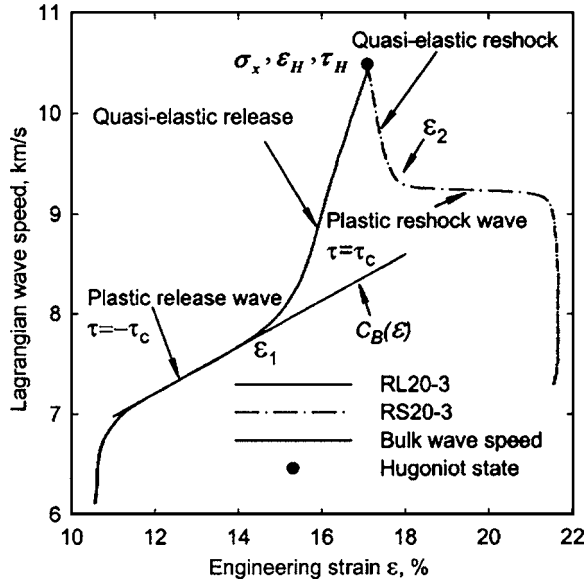

FIG. 8. Longitudinal and bulk Lagrangian wave speed measurements used for estimating the shear stress changes occurring during either quasielastic unloading or quasielastic reloading.

loading. The response of the material is quasielastic near the initial shock state, transitioning to an assumed plastic response in the lower part of the curve. During quasielastic unloading the shear stress τ decreases from a value, which we will define as τ_H ($\tau_H > 0$), as yet unknown at the shocked state, to a state on the inverse yield surface, which is represented by $-\tau_c$, and corresponds to full plastic deformation. For quasielastic reloading, the shear stress will increase from τ_H to the critical strength $+\tau_c$ on the upper yield surface.

The quasielastic portion of the wave profiles can be used to directly determine the longitudinal wave speeds C_L needed for Eq. (8). The bulk wave speed C_B over the region of quasielastic response for both cases is required in Eq. (8) and was evaluated from the plastic part of the release wave profile, as shown in Fig. 8, by extrapolating the response for the lower part of the profile, which is assumed to represent bulk response. Furthermore, this extrapolation was also used to estimate C_B for quasielastic reloading before the arrival of the plastic wave. This approach is thought to introduce negligible errors in estimating the shear stress.

Integrating Eq. (8) in both the quasielastic reshock and release regions and noting that the shear stress τ varies in the range of (τ_H, τ_c) and ε varies in $(\varepsilon_H, \varepsilon_2)$ during reshock, and differently in the release process $(\tau_H, -\tau_c)$ and $(\varepsilon_H, \varepsilon_1)$, where $\varepsilon_H < \varepsilon_2$, but $\varepsilon_H > \varepsilon_1$ gives the following relations:[6]

$$\text{Release experiment:} \quad \tau_c + \tau_H = -\frac{3}{4}\rho_0 \int_{e_1}^{e_H} (C_L^2 - C_B^2)\, d\varepsilon, \tag{9a}$$

$$\text{Reshock experiment:} \quad \tau_c - \tau_H = \frac{3}{4}\rho_0 \int_{e_H}^{e_2} (C_L^2 - C_B^2)\, d\varepsilon. \tag{9b}$$

As discussed earlier, Eqs. (9a) and (9b) allow estimates of the shear stress τ_H at the shocked state and the critical shear strength τ_c.

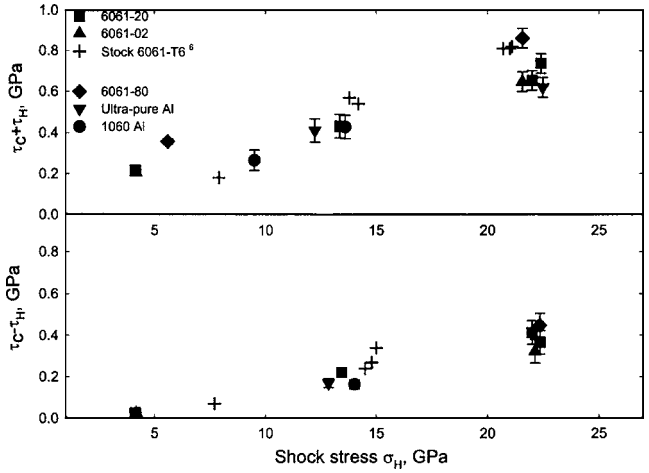

FIG. 9. Shear stress data measured in reshock and release experiments. The quantities $\tau_c + \tau_H$, $\tau_c - \tau_H$ were estimated from reshock and release experiments, respectively.

F. Shear strength results

The results of $\tau_c + \tau_H$ from release experiments and $\tau_c - \tau_H$ from reshock experiments are listed in Table II. In several cases, the initial Hugoniot stress was not identical for both sets of experiments, so that an average is used to represent the initial shock stress. The measured values of $\tau_c + \tau_H$ and $\tau_c - \tau_H$ are plotted in Fig. 9, along with previous data reported for as-received 6061-T6.[6] The shear strength τ_c and shear stress τ_H at the shocked state were determined from the measured data and are plotted in Figs. 10 and 11 as a function of σ_H.

At 4 GPa, three data points for shear strength from 6061-20 to 6061-02 are identical to within experimental error. The inferred shear strength of 6061-02 (<5-μm grain size) is similar to that for 6061-20 (30-μm grain size) for stresses of 4–22 GPa. Note also from Table II that strength measurements on different sample thickness of 6061-20 are similar. However, the shear strength of the 50-μm grain aluminum material, 6061-80, is slightly larger than that for the

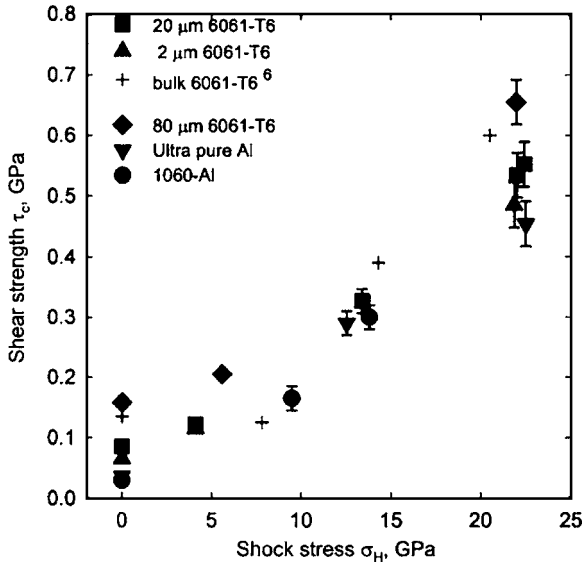

FIG. 10. Shear strength τ_c of the different aluminum materials.

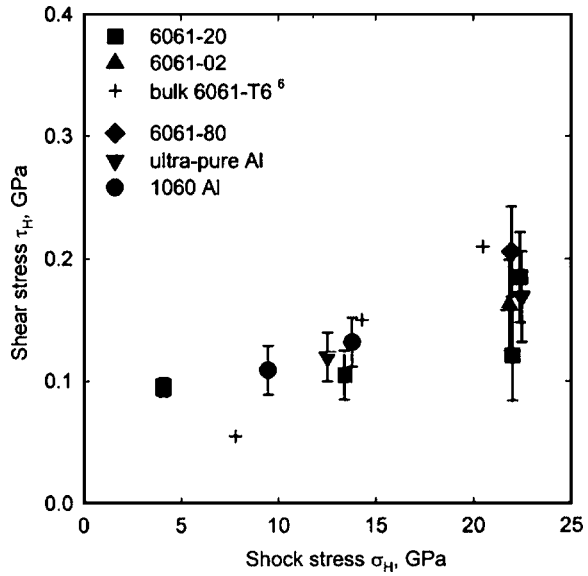

FIG. 11. Shear stress τ_H of the different aluminum materials.

smaller grained materials and very similar to that for as-received stock 6061-T6.[6] As shown in Fig. 10, there is a clear trend between the strength of the different materials and the initial yield strength, or HEL. The maximum spread in strength is small, about 0.2 GPa, but is certainly larger than the expected error bar of less than 0.1 GPa which is discussed below. Essentially, at a Hugoniot stress of 22 GPa, it is observed that the smaller grain sizes of 6061-T6 have lower strength. However, it should be kept in mind that the 6061-02 and 6061-20 aluminum samples also have a lower HEL, which will be important as we will show.

At a shock stress of approximately 13 GPa, four data points were obtained for four different aluminum materials. The pure Al 1060, ultrapure Al, and 6061-20 materials have essentially the same shear strength, even though the impurity levels and grain sizes are different, and also comparable results with 6061-T6 at a slightly higher stress. This comparison provides further evidence about shock-induced deformation mechanisms that influence compressive strength. Details of grain size, impurity levels, and whether impurities are in solid solution or as precipitates, which are known to control material strength at quasistatic uniaxial stress loading conditions, appear to have a negligible effect on strength properties under intense shock loading.

Additional experiments were conducted on 6061-80 and 1060 aluminum at 5.7 and 9.5 GPa to investigate whether a possible threshold of compression for shear strength exists as previously suggested.[6] However, the present data strongly suggest that a critical threshold for hardening does not exist and that the hardening varies smoothly over the stress range studied. This observation has strong implications for modeling the strength variation, as we will show.

The results in Fig. 11 conclusively show that the shear stress τ_H in the shocked state is less than the shear strength τ_c at the same shock stress. There appears to be a definite increase in τ_H from its initial value τ_0. Figure 11 illustrates an increase of 0.1–0.18 GPa, which is larger than experimental error bars.

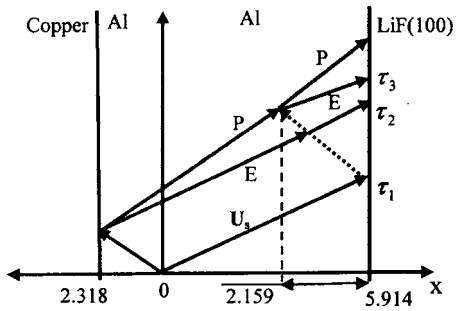

FIG. 12. Schematic *x-t* diagram for wave interaction in the target for reshock experiment RS20-3, where the reshock wave was disturbed in the region of 2.159 mm to the target/window interface. This causes a slight perturbation to the following plastic wave since a new elastic wave is formed at that interaction.

As discussed earlier, two principal mechanisms have been proposed to explain the apparent time-dependent effects of yielding. If the microband model of Swegle and Grady[7] applies, the shear stress τ_H should decrease with applied shock amplitude because of the greater local temperatures expected. In contrast, the shear stress τ_H shown in Fig. 11 increases with σ_H and would be more compatible with a stress distribution model.[4] However, due to wave interactions produced by heterogeneous deformation, the resulting shear stress τ_H could easily be proportional to the shock stress, as suggested by Fig. 11, which would tend to suggest the model of Lipkin and Asay.[4]

G. Analysis of systematic and random errors

Although the impedance mismatch between Al and LiF (100) is small, on the order of 2%, it can have a major effect in reshock experiments. Since the impedance of LiF is slightly less than that for aluminum, a release wave originating from the first shock-window interaction will elastically unload the sample to a state within its yield surface. Recompression from this perturbed state will result in elastic response, as illustrated by the region to the right of the dashed line in Fig. 12. Experiments were designed so that the amount of material perturbed by this reflection is minimized. Also, note that if a quasielastic recompression does not actually occur, the reflected elastic unloading from τ_1 will still interact with the following plastic wave, indicated by the line P in Fig. 12, resulting in the formation of a small elastic recompression that leads to the plastic recompression. This effect was investigated in detail, as discussed below.

A one-dimensional (1D) wave propagation code COPS (Ref. 45) was used to simulate a specific experiment in order to estimate the systematic error arising from the impedance mismatch in the measured values of $\tau_c - \tau_H$ listed in Table II. An elastic-plastic model with strain hardening was used in the simulation, which produces only plastic recompression from the shocked state. A calculation performed for the RS20-3 experiment at 22 GPa, as illustrated in Fig. 13, shows a small ramp reloading, originating from the interaction of the reflected elastic wave and the plastic recompression wave. This produces a small elastic reflection as shown in Fig. 12, which arrives at τ_3 before the main plastic reshock. If this perturbation were misinterpreted as arising

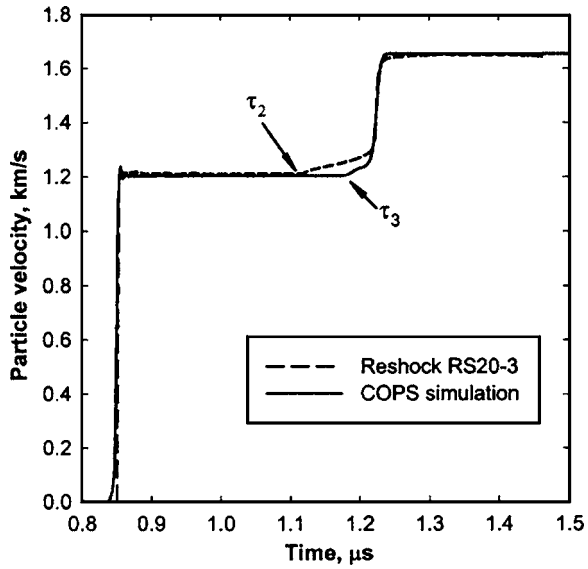

FIG. 13. A relative small apparent quasielastic response arises from a target/window impedance mismatch when the window has a lower impedance than the target. The dashed profile shows the actual measured profile for experiment RS20-3 and the solid line corresponds to a 1D simulation with an elastic-plastic model. The perturbation results from the wave interaction in Fig. 12, forming a new elastic wave by the interaction of the reflected elastic unloading and the plastic reloading.

from the aluminum-copper interface, the apparent wave speed would be considerably lower than measured in the experiment. Its amplitude is also considerably smaller than measured, as observed in Fig. 13. This calculation indicates that although a certain level of "apparent" elastic response can arise from an impedance mismatch between the sample and window, the dominant response observed in the present experiments is due to the characteristic response of the material to reloading. The impedance mismatch effect can be minimized by designing the experiment to keep the recompression wave-perturbation interaction near the window interface. In the present experiments, this interaction region was maintained to about one quarter of the sample thickness on the window side.

To demonstrate that the window perturbation produces a negligible error in shear stress estimates for unloading experiments, a quasielastic release wave model[46] was used in COPS to realistically simulate the measured release wave profiles. Calculations based on known EOS properties were performed for both the LiF (100) window and replacement of LiF with an Al window, keeping all other properties the same. These simulations showed that the release wave produced at the target/window interface overlapped after corrections for the different EOS properties of the Al and LiF windows. These comparisons demonstrated that the impedance mismatch produces a larger error for the quasielastic reshock than for the quasielastic release. Thus, no apparent systematic error from the mismatch impedance was observed for $\tau_c+\tau_H$ evaluated from quasielastic release waves. Although this effect should not be a problem in the present experiments, ignoring the impedance mismatch for larger differences in shock impedance would lead to much larger errors.

Calculations of $\tau_c-\tau_H$ were performed to estimate the systematic error in reloading experiments. The systematic

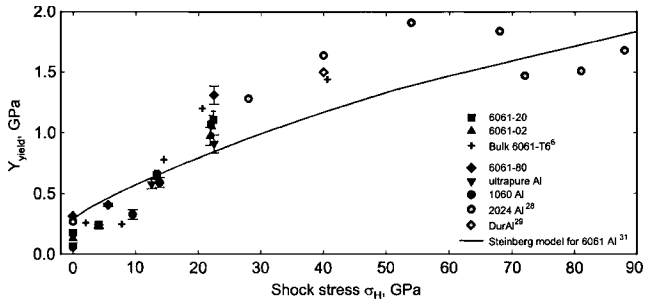

FIG. 14. Strength of shocked aluminum materials compared with the results of the Steinberg-Guinan strength model for 6061-T6.

errors arising from the impedance mismatch in estimating τ_c and τ_H are in opposite directions; for example, the error for $\Delta\tau_c$ is $-0.5\Delta\delta$, and for $\Delta\tau_H$ is $0.5\Delta\delta$, where $\Delta\delta$ is the magnitude of $\tau_c-\tau_H$. At 22 GPa, it was found that $\Delta\delta=0.080$ GPa, which is about 20% of that estimated from VISAR wave profiles, and at 13 GPa, $\Delta\delta=0.013$ GPa, which is about 6% of that listed in Table II. The larger relative error in $\Delta\tau_H$ is due to the systematic error from impedance mismatch, which is larger than that for unloading. We have not attempted to correct the measured stresses for these systematic errors, although they should be kept in mind for comparisons with results from other techniques or in modeling.

In addition to the systematic error described above, there are several sources of random errors that range from sample preparation to wave profile analysis. The major contributions are measurements of projectile velocity, VISAR particle velocity, and Lagrangian longitudinal and bulk wave speeds. A detailed analysis was performed by the quadrature summation of each source of uncertainty to estimate the overall random error. The relative accuracy of VISAR particle velocity measurements is 0.2% at 4 GPa and 1% at 22 GPa experiments;[38] shock wave velocity has an uncertainty of ~1%; the Lagrangian wave speed uncertainty is about 1.1%; the relative error for engineering strain is approximately 0.2%; and the Hugoniot stress uncertainty is about 2%. The resulting random error for shear strength τ_c is about 4%, 7%, and 7% at 4, 13, and 22 GPa, respectively. For the shear stress τ_H, the estimated uncertainty is about 5%, 10%, and 18% for 4, 13, and 22 GPa, respectively.

IV. DISCUSSION OF THE YIELD STRENGTH OF ALUMINUM AT HIGH SHOCK STRESSES

Values of the yield strength ($Y=2\tau_c$) for various pure and aluminum alloys are plotted in Fig. 14. Similar measurements on 2024 Al and duraluminum obtained at high shock stresses are also included in the figure.[28,29]

Although the metallurgical properties of the eight aluminum materials shown vary considerably, the strength data follow similar trends from zero stress to approximately $\sigma_H=55$ GPa, except for the four points at stresses greater than 65 GPa, where temperature effects and measurement error may be enhanced. The various materials exhibit different values of yield strength at ambient conditions from 0.058 to 0.27 GPa, as illustrated in Fig. 10. These variations result from different metallurgical characteristics that control

the initial strength. Under shock loading, these differences are approximately preserved, resulting in the variation shown in Fig. 14.

Specific descriptions of these variations are as follows. There are five experiments at stress levels of 2.5–7.9 GPa that produce strength values of about 0.24 GPa. The yield strength for 1060 Al at 9.5 GPa shows a definite increase over the lower-stress values. The three data points near 13 GPa on 6061-20, 1060 Al, and ultrapure Al samples show a slight but definite correlation of shock-induced and ambient strengths. The neighboring data obtained on stock 6061-T6 (Ref. 6) are higher but show the same trend. The several data points for various aluminum materials near 22 GPa show larger scatter but again correlate with the ambient strength. The strength data for 2024 alloy show a similar trend for shock states greater than 22 GPa. One data point obtained on duraluminum (~6061-T6 Al) at 40 GPa indicates similar strength to 2024 Al at the same shock stress.[28] The data on 2024 indicate deviation from the increasing trend at shock levels near 68 GPa even though the data were reported by a different author.

It should be noted in Fig. 14 that strength data are plotted as a function of shock stress but this does not imply that σ_H is the controlling parameter. For example, an increase in σ_H is accompanied by increases in both the plastic strain and the mean stress, or pressure, so that any of these variables could equally be used to show the trend in the data. In any case, the large number of materials represented and the large range of strength data make a compelling argument for yield strength increasing smoothly with shock stress over the range of 0–55 GPa, with individual data points deviating locally in accordance with their initial yield strength.

Various material models have been developed to describe strength variations under dynamic loading.[30,31,47–49] The Steinberg-Guinan model is commonly used for shock wave loading since it provides a convenient representation of strain hardening, pressure, and temperature dependence that can be determined from other experiments. In this model, the yield strength Y can be written in the form

$$Y = Y_0[1+\beta(\varepsilon_p+\varepsilon_i)^n]\left[1+\left(\frac{G_P'}{G_0}\right)\frac{P}{\eta^{1/3}}-\left(\frac{G_T'}{G_0}\right)(T-300)\right], \tag{10}$$

where Y_0 is the initial yield stress, ε_p is the current plastic strain, $\varepsilon_i \approx 0$, is the plastic strain at the HEL, work hardening is described by the factors β and n, η is the volume compression, $\eta = V_0/V = \rho/\rho_0$, and G is the shear modulus at the corresponding pressure and temperature, with derivatives indicated by a prime. For 6061-T6 aluminum, Steinberg reports these parameters as $Y_0 = 0.29$ GPa, $\beta = 125$, $n = 0.1$, $G_P'/G_0 = 0.0652$/GPa, and $G_T'/G_0 = 6.16 \times 10^{-4}$/K.

The parameters given above were used to estimate the shock stress dependence of the yield strength using estimated shock temperatures from McQueen *et al.*;[50] the resulting curve is plotted in Fig. 14 for comparison with experimental results. The Steinberg-Guinan model reproduces the general behavior, in that it roughly follows the experimental data from ambient to shock stresses of 90 GPa. However, the model shows significant variations from experimental results, both for stresses below 13 GPa and for data at high-stress levels. Part of the observed deviation is due to the fact that the Steinberg-Guinan model was developed from unloading data alone, which is insufficient to estimate the yield stress in the shocked state.

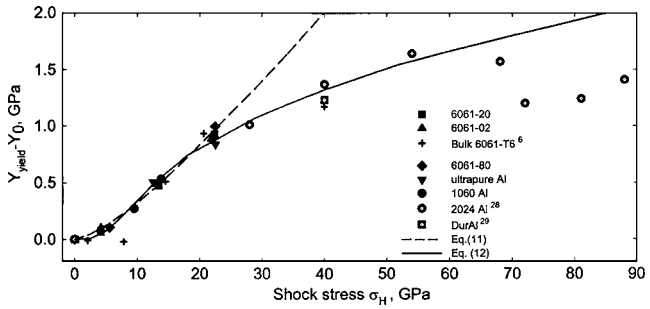

FIG. 15. The increased in yield strength ΔY_{yield} of various aluminum materials and the strength calculations.

As illustrated in Figs. 10 and 14, there appears to be a correlation with shock-induced strength variations and the initial values. This observation suggests that the initial yield strength may simply be an addition to the increase in strength resulting from a combination of plastic strain and pressure hardening. This hypothesis motivates the plot of Fig. 15, which presents only the change in yield strength for all materials shown in Fig. 14. This figure demonstrates that the change in strength follows the same trend as in Fig. 14, but with much less data scatter, except for a single point on stock 6061-T6 at 7.9 GPa.[6] A continuous increase is observed to a stress level of 55 GPa, which is an important observation and suggests that the high-stress response of all aluminum materials represented in the figure follows a similar dependence on stress. There are a few additional data reported for 6061-T6 and pure aluminum for stress levels beyond 40 GPa that are not shown in the figure, since they were obtained with a technique that has not been fully validated,[51] the data are not consistent with previous reported data for 6061-T6 at 40 GPa, and only unloading data were reported so a good estimated of strength is not possible.

The relationship of compressive strength data to shock stress illustrated in Fig. 15 provides motivation for a model of shock-induced strength. It is well known that the initial yield strength is strongly dependent on metallurgical properties, as verified in a large number of low-rate, low-stress applications, including the Hugoniot elastic limit. However, the present results strongly suggest that the initial strength, and presumably the initial metallurgical properties, do not play a significant role at high shock stresses. Based on this observation, we developed a strength formulation that describes only the change in yield strength ΔY due explicitly to shock compression. The resulting model calculation is shown in Fig. 15 and is observed to represent the response of all eight materials very well. The pressure hardening and temperature softening terms previously developed by Steinberg *et al.* in Eq. (10) were retained without modification, since they should be an inherent property of aluminum. To fit the data shown in Fig. 15, a two-parameter strain hardening term was used,

$$\Delta Y = \beta \varepsilon_P{}^n \left(1 + A\frac{P}{\eta^{1/3}} - B\Delta T \right), \tag{11}$$

where $A = G'_P/G_0^-$, $B = G'_T/G_0$, and $\Delta T = T - 300$. As shown by the dashed curve in Fig. 15 using values of β and n as $\beta = 8.726$ GPa and $n = 1.376$ fits the present data and the data of Asay and Chhabildas very well to 22 GPa, but not the data above that stress level. However, relation (11) should accurately represent the present data at any intermediate stress over this range; the reported data above 22 GPa are highly uncertain since they are based on unloading data alone. We have not attempted to correct the reported data at higher stresses. Estimation based on extrapolation of our recompression data to 50 GPa indicates that the yield strength could be as high as 2.8 GPa. This issue should be resolved in future experiments by combining unloading and reshock experiments, as done in the present study.

To simulate the higher-stress amplitudes in Fig. 15, a three-parameter function for plastic strain hardening term was developed, resulting in the following equation:

$$\Delta Y = \frac{a}{1 + (\varepsilon_P/b)^n} \left(1 + A\frac{P}{\eta^{1/3}} - B\Delta T \right), \tag{12}$$

again assuming the earlier parameters for A and B. The constants a, b, and n were adjusted to fit the full range of data, resulting in $a = 0.484$ GPa, $b = 0.0692$, and $n = -3.0411$. The results are plotted in Fig. 15 as the solid line. The relation fits the whole set of data, including the present data and the data on 2024 and duraluminum alloys to within experimental error.

The phenomenological model represented by Eq. (12) indicates that the yield response has three distinct regions: (1) for stresses less than 5 GPa, ΔY increases slowly with pressure and about 80% of the total increase results from plastic strain hardening; (2) for stresses between 5 and 18 GPa, ΔY rapidly increases with pressure. At 18 GPa, plastic strain and pressure hardening contribute about equally; and (3) from 18 to 55 GPa, both pressure and temperature are dominate terms, with decreasing rate, suggesting the increasing importance of temperature. The plastic strain hardening contribution is about 30% at $\sigma_H = 50$ GPa.

Equation (12) suggests that the initial compressive strength and resulting HEL do not strongly affect the change in strength due to shock loading at high stresses. This tentative conclusion is significant since it implies that even though initial metallurgical properties control material strength at lower loading rates including possibly lower shock amplitudes, they are not dominant at high loading rates and shock stresses where deformation mechanisms produced by the shock itself may dominate. The implication is that deformation of the aluminum matrix dominates shock hardening, not grain size, impurities, precipitates, or other defects. Although these hardening mechanisms cannot be identified from the present data, they could include grain boundaries where dislocation pileups occur,[52–54] conjunctions of dislocation slip planes where dislocations become pinned,[52,53] and the pressure dependence of the shear modulus.[30] Even though Eq. (12) is phenomenological, it explicitly indicates the relative contribution of each hardening source to the change ΔY which is instructive for designing experiments to identify the relative contributions of plastic strain. The effects of grain boundary and conjunctions of main slip planes could also be separated experimentally. The explicit contribution of grain-boundary effects cannot be unambiguously evaluated from the present experiments, although the grain size and thus the grain-boundary density are definitely different for the various materials. Shock wave experiments on single-crystal aluminum would be useful in identifying the importance of grain boundaries to shock-induced hardening. Additional experiments to separate strain and pressure hardening effects would also be useful for further evaluation of Eq. (12).

As we discussed earlier, mesoscale models based on either localized temperature generation in hot spots during shock loading[7,8] or a distributed shear stress model[4,27] were previously developed to explain the observed quasielastic recompression results. All materials studied in the present experiments were polycrystalline, although grain sizes and impurities varied substantially between materials. With only the observation that the change in compressive strength from ambient is similar for different materials, it is not possible to differentiate between the two models. However, measurements of yield strength in materials compressed to the same levels with nonshock, or quasi-isentropic loading, or in single-crystal material aluminum without grain boundaries would be useful in differentiating between the mechanisms. Strength information under isentropic loading is presently extremely limited, although some data have been reported for aluminum, tantalum, and tungsten.[10,23,55–57]

The present research has implications for determining strength using other techniques and for strength data on different materials. Often, strength data are extracted from unloading wave profiles, which results in the quantity $\tau_c + \tau_H$. The combined recompression and unloading results show that unloading data alone can result in the substantial error in estimating compressive strength. For example, Fig. 9 illustrates that use of only the unloading profiles alone would result in an apparent compressive strength that is about 25% too low at a shock stress of 20 GPa. Neglect of the shear stress effects occurring during recompression would thus result in a systematic error in estimating strength. Although the present results concern shock loading, unloading, and reloading of aluminum, we expect that similar results would occur in other polycrystalline materials and also for different loading conditions; e.g., ramp loading followed by unloading, or in Rayleigh-Taylor experiments[23] currently being used to estimate strength under ramp loading.

V. CONCLUSIONS

In the present experiments, a combination of shock loading followed by either unloading or reloading was used to evaluate the compressive yield strength of several aluminum materials over the first-shock stress range of 4–22 GPa. An extensive set of shock wave experiments was performed to determine the compressive strength after shock compression and to evaluate the effects of initial metallurgical properties on compressive strength. To accomplish this, three different

grain sizes of 6061 aluminum alloy were studied with the average size ranging approximately from <5 to 50 μm and for heat treatments approximately in the T6 condition. Two pure aluminum materials were also studied, which included commercially pure 1060 aluminum alloy (99.5% Al) with a grain size of about 180 μm and ultrapure aluminum (99.9998% Al) with an average grain size of about 300 μm.

Strength information in the shock-compressed state was extracted from a combination of unloading and reloading experiments. In both cases, quasi-elastic-plastic response was observed, which is not expected from elastic-plastic theory and is anomalous from that perspective. The present observations of quasi-elastic-plastic response are consistent with previously reported results.[4,6]By comparing measured strength results on materials with different grain sizes but similar composition, it was found that grain size is at most a minor contribution to compressive strength at a high shock compression. Also, by comparing results from alloys with a large amount of impurities or inclusions with relatively pure aluminum, it was found that impurities and inclusions are not a dominating factor for yield strength.

A major observation is that the compressive strength for all materials studied increases significantly with the same dependence on shock stress. The essential differences between the different alloys and pure aluminum result from the differences in their initial yield strengths. The shock-induced yield strength for a hard alloy with an initial large yield strength and therefore a high HEL is offset from that for a softer material at the same stress level by roughly the difference in initial yield strengths. This is a significant result that considerably simplifies modeling, since detailed metallurgical properties apparently do not dominate yield response under intense shock loading. To clarify the dependence of yield strength on plastic strain, pressure, and temperature under shock loading, the Steinberg-Guinan model[31] was first used to compare with the data. Using parameters reported for 6061-T6 it was found that this model reproduces the observed increase of yield strength with shock amplitude in general terms but varies substantially in the details. It overestimates the measured strength at shock stresses to about 13 GPa and underestimates it for higher stresses.

To obtain closer agreement with experimental data, a strength model was developed to describe only the change in yield strength from its ambient value and a functional form for the plastic strain dependence was developed to fit the measured strength data. For these fits, the pressure and temperature dependences previously proposed by Steinberg *et al.* were preserved. It was found that this relation accurately describes the present data as well as other strength data, including 2024 aluminum alloy and duraluminum, to shock stresses of about 55 GPa. The model exhibits three regions of hardening: a low-stress region where plastic work hardening dominates; a stress region beginning near 5 GPa where the rate of pressure hardening significantly increases and both plastic strain and pressure play a major role; and a region above about 18 GPa where notable softening effects arise and temperature effects become important.

The model suggests that the strength of aluminum increases with both plastic strain and shock stress, but that the change is independent of metallurgical properties that control the initial strength. The influence of metallurgical properties on initial strength data is preserved, but the model suggests that shock-induced deformation mechanisms in the aluminum matrix dominate strength changes at high shock levels.

The present work covers an extensive set of initial material properties and presents possible correlations between initial properties and shock-induced compressive strength. However, additional work is required to examine the proposed material model in more detail, to evaluate the relative contributions of plastic strain, pressure, and temperature to the yield strength, and to differentiate between mesoscale deformation mechanisms that could account for the observed results. To this end, ramp wave or quasi-isentropic compression experiments would be useful to evaluate material strength at equivalent stress levels, but different loading rates. Shock loading/unloading/reloading experiments on single-crystal aluminum would also be useful for providing additional information on the importance of different local deformation mechanisms. Finally, cyclic loading of aluminum subjected to high shock stresses, fully unloaded and then reloaded, would be valuable for differentiating between plastic strain and pressure hardening effects.

ACKNOWLEDGMENTS

We would like to acknowledge several people who have played a key role in this research. We thank Kurt Zimmerman and Kent Perkins for their assistance in conducting the shock wave experiments and Professor Y. M. Gupta for providing overall guidance and for many helpful discussions. Erin Devlin of the Colorado School of Mines is acknowledged for preparing the different 6061 aluminum heat treatments and Mark Fuller of Microelectronics Fabrication Facility, Washington State University for plating the indium bonds necessary for high-quality reshock experiments. Many thanks to Xianglei Chen for EBSD grain-size measurements, to Sunil Dwivedi for many discussions, to Jim Johnson for technical advice, and to Professor David Field of the Department of Mechanical Engineering, Washington State University for advice on characterizing metallurgical properties. This work was supported by the U.S. Department of Energy under Grant No. DE-FG52-97SF21388.

[1] L. W. Davison and R. A. Graham, Phys. Rep. **55**, 256 (1979).
[2] G. E. Duvall and R. A. Graham, Rev. Mod. Phys. **49**, 523 (1977).
[3] G. R. Fowles, J. Appl. Phys. **32**, 1475 (1961).
[4] J. Lipkin and J. R. Asay, J. Appl. Phys. **48**, 182 (1977).
[5] J. R. Asay and J. Lipkin, J. Appl. Phys. **49**, 4242 (1978).
[6] J. R. Asay and L. C. Chhabildas, in *Shock Waves and High Strain-Rate Phenomena in Metals: Concepts and Applications*, edited by M. A. Meyers and L. E. Murr (Plenum, New York, 1981), p. 417.
[7] J. W. Swegle and D. E. Grady, in *Metallurgical Application of Shock-Wave and High-Strain-Rate Phenomena*, edited by L. E. Murr, K. P. Standhammer, and M. A. Meyers (Marcal Dekker, New York, 1986), p. 705.
[8] D. E. Grady and J. R. Asay, J. Appl. Phys. **53**, 7350 (1982).
[9] J. R. Asay, L. C. Chhabildas, and D. P. Dandekar, J. Appl. Phys. **51**, 4774 (1980).
[10] T. J. Vogler, W. D. Reinhart, and L. C. Chhabildas, J. Appl. Phys. **95**, 4173 (2004).
[11] M. N. Pavlovskii, V. S. Stepanyuk, and V. V. Komissarov, Strength Mater. **10**, 50 (1991).
[12] L. V. Al'tshuler, M. N. Pavlovskii, V. V. Komissarov, and P. V. Makrov, Combust., Explos. Shock Waves **35**, 92 (1999).

[13]R. S. Hixson and J. N. Fitz, J. Appl. Phys. **71**, 1721 (1992).
[14]P. L. Hereil, J. Phys. Colloq. **49**, 3 (1988).
[15]L. C. Chhabildas, J. L. Wise, and J. R. Asay, in *Shock Waves in Condensed Matter-1981*, edited by W. J. Nellis, L. Seaman, and R. A. Graham, AIP Conf. Proc. No. 78 (American Institute of Physics, New York, 1982), p. 422.
[16]W. D. Reinhart and L. C. Chhabildas, Int. J. Impact Eng. **29**, 601 (2003).
[17]R. J. Clifton, M. Mello, and N. S. Brar, in *Shock Compression of Condensed Matter-1997*, edited by S. C. Schmidt, D. P. Dandekar, and J. Forbes, AIP Conf. Proc. No. 429 (American Institute of Physics, Woodbury, NY, 1998), p. 521.
[18]G. Yuan, R. Feng, and Y. M. Gupta, J. Appl. Phys. **89**, 5372 (2001).
[19]R. Feng, G. F. Raiser, and Y. M. Gupta, J. Appl. Phys. **79**, 1378 (1996).
[20]G. Yuan, R. Feng, Y. M. Gupta, and K. Zimmerman, J. Appl. Phys. **88**, 2371 (2000).
[21]H. M. Simha and Y. M. Gupta, J. Appl. Phys. **96**, 1880 (2004).
[22]M. J. C. F. Millet, N. K. Bourne, Z. Rosenberg, and J. E. Field, J. Appl. Phys. **86**, 6707 (1999).
[23]K. T. Lorenz, M. J. Edwards, S. G. Glendinning, A. F. Jankowski, J. McNaney, S. M. Pollaine, and B. A. Remington, Phys. Plasmas **12**, 056309 (2005).
[24]P. F. Chartagnac, J. Appl. Phys. **53**, 948 (1982).
[25]W. C. Moss, J. Appl. Phys. **55**, 2741 (1984).
[26]M. A. Meyers and M. S. Carvelho, Mater. Sci. Eng. **24**, 131 (1976).
[27]T. J. Vogler and J. R. Asay, in *Shock Compression of Condensed Matter-2003*, edited by M. D. Furnish, Y. M. Gupta, and J. W. Forbes, AIP Conf. Proc. No. 706 (American Institute of Physics, Melville, NY, 2004), p. 617.
[28]C. E. Morris, J. N. Fritz, and B. L. Holian, in *Shock Compression of Condensed Matter-1981*, edited by W. J. Nellis, L. Seaman, and R. A. Graham, AIP Conf. Proc. No. 78 (American Institute of Physics, New York, 1982), p. 382.
[29]*Methods for the Study of Substance Properties Under Intensive Dynamic Loading*, edited by M. V. Zhernokletov (Federal Governmental Unitary Enterprise, Sarov, 2004).
[30]D. J. Steinberg, S. G. Cochran, and M. W. Guinan, J. Appl. Phys. **51**, 1498 (1980).
[31]D. J. Steinberg, Technical Report No. UCRL-MA-106439 Change 1, Lawrence Livermore National Laboratory, 13 February 1996 (unpublished).
[32]*Electron Backscatter Diffraction in Material Science*, edited by A. J. Schwartz, M. Kumar, and B. L. Adams (Academic, New York, 2000).
[33]H. J. Kleebe (private communication).
[34]E. Devlin (private communication).
[35]G. R. Fowles, G. E. Duvall, J. R. Asay, P. Bellamy, F. Feistmann, D. E. Grady, T. Michaels, and R. Mitchell, Rev. Sci. Instrum. **41**, 984 (1970).
[36]S. C. Jones and Y. M. Gupta, J. Appl. Phys. **88**, 5671 (2000).
[37]J. L. Wise and L. C. Chhabildas, in *Shock Waves in Condensed Matter*, edited by Y. M. Gupta (Plenum, New York, 1986), p. 441.
[38]L. M. Barker and R. E. Hollenbach, J. Appl. Phys. **43**, 4669 (1972).
[39]L. M. Barker and K. W. Schuler, J. Appl. Phys. **45**, 3692 (1974).
[40]W. J. Carter, High Temp. - High Press. **5**, 313 (1973).
[41]R. Feng and Y. M. Gupta, Shock Dynamic Center Internal Report No. 94–01, 1994 (unpublished).
[42]W. J. Nellis, A. C. Mitchell, and D. A. Young, J. Appl. Phys. **93**, 304 (2003).
[43]H. Conrad and G. Schoeck, Acta Metall. **8**, 71 (1960).
[44]G. E. Duvall (private communication).
[45]Y. M. Gupta, COPS Wave Propagation Code, SRI International, 1976.
[46]J. N. Johnson, R. S. Hixson, G. T. Gray III, and C. E. Morris, J. Appl. Phys. **72**, 429 (1992).
[47]G. R. Johnson and W. H. Cook, Eng. Fract. Mech. **21**, 31 (1985).
[48]D. L. Preston and D. L. Tonks, J. Appl. Phys. **93**, 211 (2003).
[49]F. J. Zerilli and R. W. Armstrong, J. Appl. Phys. **68**, 1580 (1990).
[50]R. G. McQueen, S. P. Marsh, J. W. Taylor, J. N. Fritz, and W. J. Carter, in *High-Velocity Impact Phenomena*, edited by R. Kinslow (Academic, New York, 1970).
[51]J. R. Asay, L. C. Chhabildas, G. I. Kerley, and T. G. Trucano, in *Shock Waves in Condensed Matter-1985*, edited by Y. M. Gupta (Plenum, New York, 1986), p. 145.
[52]J. Weertman and J. R. Weertman, *Elementary Dislocation Theory* (The Macmillan Company, New York, 1964).
[53]R. W. K. Honeycombe, *The Plastic Deformation of Metals*, 2nd ed. (Edward Arnold, Australia Pty Ltd. 1984).
[54]M. A. Meyers, D. J. Benson, O. Vöhbringer, B. K. Kad, Q. Xue, and H.-H. Fu, Mater. Sci. Eng., A **322**, 194 (2002).
[55]L. C. Chhabildas and J. R. Asay, in *Shock-Wave and High-Strain-Rate Phenomena in Materials*, edited by M. A. Meyers, L. E. Murr, and K. P. Staudhammer (Marcel Dekker, New York, 1992), p. 947.
[56]L. M. Barker, in *Shock Waves in Condensed Matter-1993*, edited by J. R. Asay, R. A. Graham, and G. K. Straub, (Elsevier Science, B. V., New York, 1984), p. 217.
[57]T. J. Vogler, *Shock Waves in Condensed Matter* (to be published).